Sensitivity Analysis of the Wind Farm High Frequency Resonance under Transmission Cable Resistance Variation

Yipeng Song, Esmaeil Ebrahimzadeh, Frede Blaabjerg
Department of Energy Technology, Aalborg University, Aalborg, Denmark
yis@et.aau.dk, ebb@et.aau.dk, fbl@et.aau.dk

***Abstract* - The High Frequency Resonance (HFR) of the Doubly Fed Induction Generator (DFIG)-based wind farm is possible to occur when the wind farm is connected to the long-distance transmission cable. The cable resistance may always be in variation due to temperature and humidity changing, insulation condition variation and etc. In this paper, it is found out that the amplitude of the HFR is influenced by the cable resistance, thus it is interesting to investigate the HFR performance under various cable resistance. The impedance modeling of the DFIG-based wind farm and the long-distance transmission cable are established first, then the HFR will be analyzed under the variation of the transmission cable resistance using the Nyquist based method. Time domain simulation results based on MATLAB/Simulink are provided to validate the analysis.**

Keywords— DFIG based wind farm; long distance transmission cable; high frequency resonance; sensitivity analysis.

I. INTRODUCTION

The wind power generation technology has been under rapid growth during the past decades, and emerging advanced control strategies have been developed to deal with the grid low voltage fault [1], to provide grid frequency support [2], to improve system performance under unbalanced and distorted grid voltage [3]-[6].

The Sub-Synchronization Resonance (SSR) [7]-[11] in the Doubly Fed Induction Generator (DFIG) based wind farm may occur due to the series compensated long distance transmission cable. The SSR has been under intensive investigation during the past few years, and several active damping strategies have been developed to suppress the SSR and ensure the safe and reliable operation of the power grid and transmission system.

Beside the SSR, for the conventional wind power plant connected to the High Voltage AC (HVAC) grid, the DFIG-based wind farm is always connected to the grid through long-distance AC transmission cables. Due to the existence of the power factor capacitors and the parasite capacitors between the cable and the ground, the transmission cables may be parallel compensated [12]-[13], this indicates an equivalent capacitors between the cable and the ground, thus the High Frequency Resonance (HFR) may occur under this circumstance [12]-[13] due to the impedance interaction between the DFIG based wind farm and the transmission cable.

For the purpose of accurately determining the occurrence of the HFR, the impedance modeling of the long distance transmission cable in the HVAC transmission needs to be precisely established [14]. Unlike the previous works where the series compensated or parallel compensated cable modeling is adopted, the cable impedance in this paper is modelled as the series connection of several Π units [14], which contain the Resistance (R) and Inductance (L) components in series as well as the Capacitance (C) components in both ends within each single Π unit. It should be noted that in practical applications, the transmission cable resistance may always be in variation due to the temperature and humidity changing, insulation condition variation and etc. The increasing of the resistance helps to achieve better damping of the resonance, and even in certain cases help to mitigate the potential resonance, while smaller resistance may comparatively aggravate the resonance. Therefore, it is meaningful to investigate the influence of the cable resistance on the HFR performance. Furthermore, in order to analyze the HFR, the impedance modeling of the DFIG based wind farm also needs to be built up [15]-[19]. This impedance modeling will be briefly illustrated in the following discussion.

In this paper, the impedance modeling of both the DFIG-based wind farm and the long-distance transmission cable are built up at first in Section II and III respectively. Then, the theoretical analysis of the HFR is conducted using the Nyquist diagram method with the consideration of the transmission cable resistance variation in Section IV. The simulation results based on MATLAB/Simulink using three different cases of cable resistance are provided in Section V to validate the analysis. Finally, the conclusions will be given in the last section.

II. IMPEDANCE MODELING OF DFIG-BASED WIND FARM

Before discussing the HFR in the DFIG system, it is important to give a brief introduction to the overall system

diagram. Fig. 1 shows the diagram of the DFIG based wind farm connected to the long transmission cable. The DFIG based wind farm contains 200 DFIG units which include Rotor Side Converter (RSC), DFIG machine, Grid Side Converter (GSC) and LCL filter. The parameters of the DFIG system are listed in Table I. The three terminal 690 V transformer is adopted to unify the output of both the DFIG machine and LCL filter. Then, the stepping-up transformer of 690 V/33 kV is applied to form the 33 kV AC bus to collect all the power delivered by the DFIG unis. Thereafter, the 33 kV/150 kV transformer is adopted to increase the voltage up to transmission level, and the long distance transmission cable at 150 kV, whose impedance is to be analyzed in this paper, is implemented. In practical applications, the length of 150 kV cable could be around 10 km to 50 km. In this paper, the typical length to be discussed is chosen to be 20 km as an example.

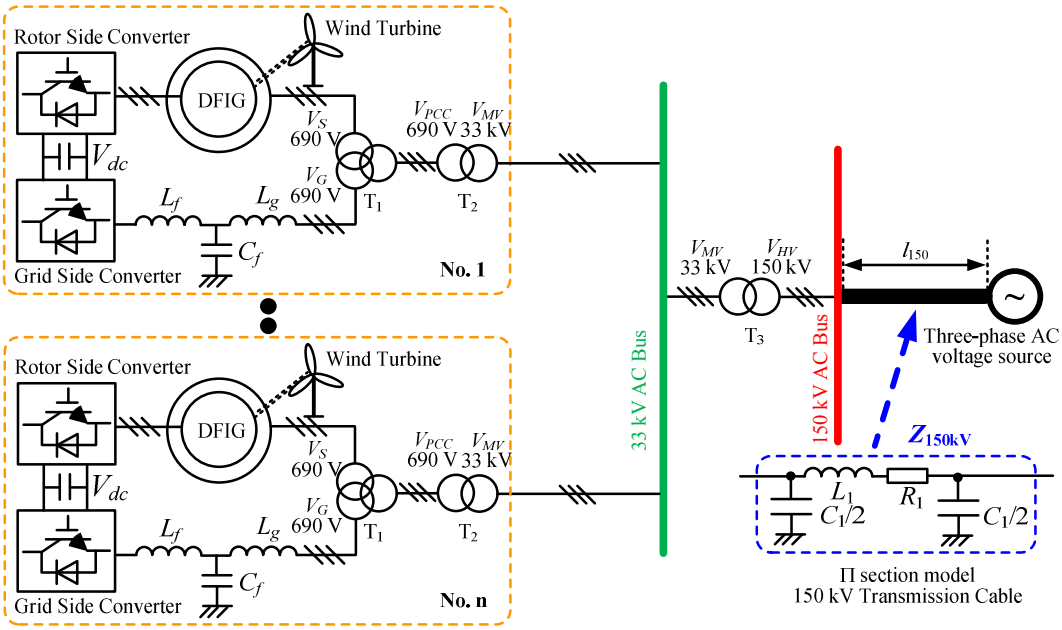

Fig. 1. Diagram of the DFIG based wind farm connected to the transmission cable

TABLE I. PARAMETERS OF DFIG BASED WIND FARM AND LONG TRANSMISSION CABLES

DFIG generator			
P_{nom}	2 MW	T_d	300 μs
R_s	0.0015 Ω	R_r	0.0016 Ω
$L_{\sigma s}$	0.04 mH	$L_{\sigma r}$	0.06 mH
L_m	3 mH	Pole Pairs	3
f_s	5 kHz	f_{sw}	2.5 kHz
LCL filter			
L_g	125 μH	L_f	125 μH
C_f	220 μF		
Current Controller Parameters in RSC and GSC			
K_{prsc}	0.08	K_{irsc}	2
K_{pgsc}	0.08	K_{igsc}	2
Voltage level			
V_G	690 V	V_{SR}	690 V
V_{PCC}	690 V	V_{MV}	33 kV
V_{HV}	150 kV		
Transmission cable			
L_0	0.4 mH/km	*number*	6
C_0	0.14 μF/km	L_{single}	5 km
R_0	89.0, 133.5, 178 mΩ/km		

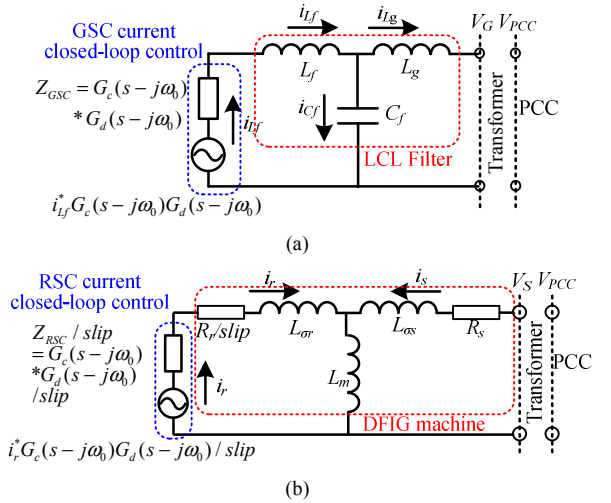

Fig. 2. Impedance modeling of (a) grid side converter with LCL filter; (b) rotor side converter with DFIG machine

The impedance of the GSC and LCL filter in the stationary frame can be obtained in Fig. 2(a) as [12]-[13],

$$Z_G = K_1^2 \frac{Z_{Cf}\left(Z_{Lf}+Z_{GSC}\right)+Z_{Lg}\left(Z_{Lf}+Z_{GSC}\right)+Z_{Cf}Z_{Lg}}{Z_{Cf}+\left(Z_{Lf}+Z_{GSC}\right)} \quad (1)$$

where, $Z_{Cf} = 1/sC_f$, $Z_{Lf} = sL_f$, $Z_{Lg} = sL_g$. C_f is the LCL-filter capacitance, L_f is the converter side inductance, and L_g is the LCL grid side inductance. K_1 is the voltage ratio between V_G and V_{PCC} defined as $K_1 = V_{PCC}/V_G$. $Z_{GSC} = G_c(s\text{-}j\omega_0)G_d(s\text{-}j\omega_0)$, $G_c(s\text{-}j\omega_0)$ is the PI current controller containing the proportional part K_{pgsc} and the integral part $K_{igsc}/(s\text{-}j\omega_0)$. $G_d(s\text{-}j\omega_0)$ is the digital control delay of 1.5 sample period due to the delay of sampling and PWM update.

The impedance of the RSC and DFIG [12]-[13] in the stationary frame can be obtained as,

$$Z_{SR} = K_2^2 \frac{Z_{Lm}H + (R_s + Z_{L\sigma s})H + Z_{Lm}(R_s + Z_{L\sigma s})}{Z_{Lm} + H} \quad (2)$$

where, $H = Z_{L\sigma r} + (R_r + Z_{RSC})/slip$; $Z_{RSC} = G_c(s\text{-}j\omega_0)G_d(s\text{-}j\omega_0)$, $Z_{Lm} = sL_m$; $Z_{L\sigma r} = sL_{\sigma r}$; $Z_{L\sigma s} = sL_{\sigma s}$. R_r is the rotor resistance, L_m is the mutual inductance, $L_{\sigma r}$ and $L_{\sigma s}$ are the rotor / stator leakage inductance. K_2 is the voltage ratio between V_S and V_{PCC} as defined $K_2 = V_{PCC}/V_S$. The slip angular speed can be presented as $slip = (s - j\omega_r)/s$, ω_r is the rotor angular speed.

Since the RSC and DFIG generator Z_{SR} and the GSC and LCL-filter Z_G are connected in parallel, the DFIG unit impedance Z_{dfig} can be obtained based on (1) and (2) as,

$$Z_{dfig} = K_3^2 \frac{Z_G Z_{SR}}{Z_G + Z_{SR}} \quad (3)$$

where, $K_3 = V_{MV}/V_{PCC}$.

Thereafter, the impedance of the DFIG based wind farm can be deduced on the basis of (3) as following,

$$Z_{wf} = \frac{K_3^2}{n_{DFIG}} \frac{Z_G Z_{SR}}{Z_G + Z_{SR}} \quad (4)$$

where, n_{DFIG} is the number of the DFIG system in the wind farm, and $n_{DFIG} = 200$ is applied in the discussion.

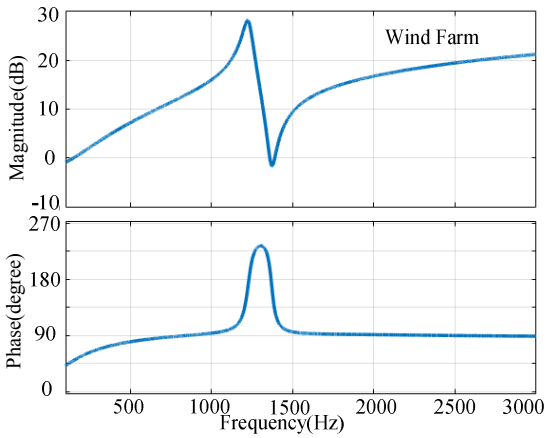

Fig. 3. Bode diagram of the impedance of the DFIG based wind farm impedance; wind farm: 200 DFIG units, total capacity of 400 MW, the parameters are listed in Table I.

Fig. 3 shows the Bode diagram of the impedance of the DFIG based wind farm. The detailed parameters of the wind farm are shown in Table I, and it is assumed there are 200 DFIG wind turbines in the farm, and the total capacity of the wind farm is 400 MW. The impedance shown in Fig. 3 is seen from the 33 kV AC bus, this indicates the inclusion of K_3 in (3).

As it can be seen from Fig. 3, the wind farm impedance is mostly inductive with the phase response of 90 degree, while the much larger phase response can be observed from 1200 Hz to 1400 Hz due to the LCL filter adopted in the GSC.

III. Impedance Modeling of the Transmission Cable

The modeling of the transmission cable has been well investigated and the Π unit based cable modeling [14] is a common solution as shown in Fig. 3. In order to better illustrate the impedance modeling of the long distance transmission cable, the one, two, three and n Π units are shown respectively in Fig. 3(a), (b), (c) and (d).

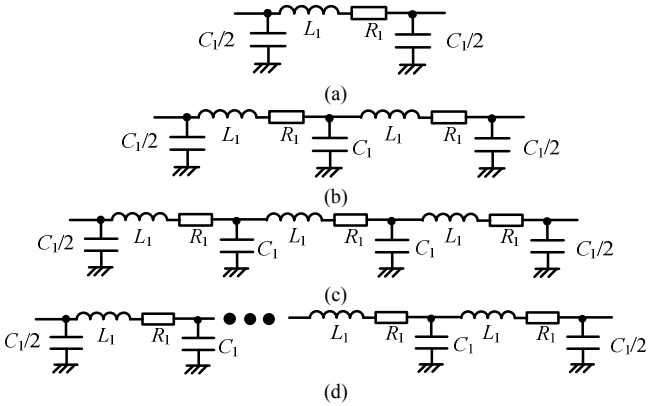

Fig. 4. Π unit based modeling of the long transmission cable (a) one Π unit; (b) two Π units; (c) three Π units; (d) n Π units;

As it can be seen, the Π unit contains the cable resistance R_1 and inductance L_1 in series connection, and the shunt capacitance $C_1/2$ between the cable and the ground. Note that R_1, L_1 and C_1 are the cable parameters of each single Π unit, and the length of each single Π unit l_{single} needs to be taken into consideration as below,

$$R_1 = l_{\text{single}} R_0; L_1 = l_{\text{single}} L_0; C_1 = l_{\text{single}} C_0; \quad (5)$$

where, R_0, C_0 and L_0 are the cable resistance, capacitance and inductance per km given in Table I.

Based on the above assumptions, the Π unit based cable modeling can be deduced as following,

1) One Π unit and its impedance expression $Z_{unit(1)}$

$$Y_{unit(1)} = \frac{1}{sL_1 + R_1} + \frac{sC_1}{2}; \; Z_{unit(1)} = \frac{1}{K_4^2 Y_{unit(1)}} \quad (6a)$$

2) Two Π units and its impedance expression $Z_{unit(2)}$

$$Y_{unit(2)} = \frac{1}{sL_1 + R_1 + \dfrac{1}{\dfrac{1}{sL_1 + R_1} + sC_1}} + \frac{sC_1}{2} = \frac{1}{sL_1 + R_1 + \dfrac{1}{Y_{unit(1)} + \dfrac{sC_1}{2}}} + \frac{sC_1}{2} \quad ; Z_{unit(2)} = \frac{1}{K_4^2 Y_{unit(2)}}$$

(6b)

3) Three Π units and its impedance expression $Z_{unit(3)}$

$$Y_{unit(3)} = \frac{1}{sL_1 + R_1 + \dfrac{1}{Y_{unit(2)} + \dfrac{sC_1}{2}}} + \frac{sC_1}{2} ; Z_{unit(3)} = \frac{1}{K_4^2 Y_{unit(3)}}$$

(6c)

4) Based on above deduction, it can be seen that the cable impedance expression is an iteration, therefore the impedance of the n Π units can be deduced on the basis of the n-1 Π units.

$$Y_{unit(n)} = \frac{1}{sL_1 + R_1 + \dfrac{1}{Y_{unit(n-1)} + \dfrac{sC_1}{2}}} + \frac{sC_1}{2} ; Z_{unit(n)} = \frac{1}{K_4^2 Y_{unit(n)}}$$

(6d)

where, $K_4 = V_{HV}/V_{MV}$ is the voltage ratio between the high voltage $V_{HV} = 150$ kV and the medium voltage $V_{MV} = 33$ kV.

Fig. 5 shows the Bode diagram of the transmission cable impedance, the cable length is 20 km, and four Π units model is adopted with the single unit length of 5 km. As it can be seen from Fig. 5, due to the existence of the capacitors between the cable and the ground at both ends of the Π units, the cable behaves capacitive above 1700 Hz, while inductive below 1600 Hz.

Due to the potential capacitive behavior of the transmission cable together with the inductive behavior of the wind farm, the HFR might occur as a consequence of the impedance interaction between wind farm and cable. This will be investigated in detail in the following discussion.

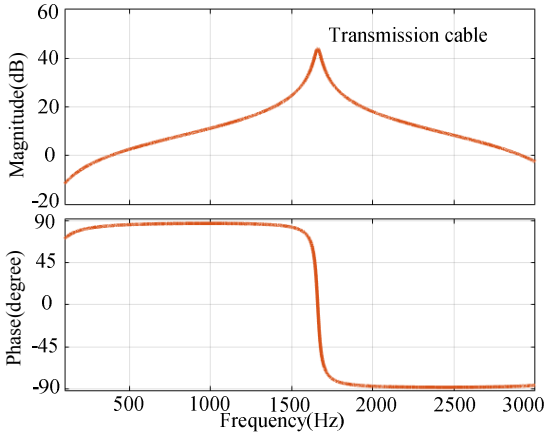

Fig. 5. Bode diagram of the transmission cable impedance, the cable length is 20 km, four Π units model is adopted with the single unit length of 5 km.

IV. Analysis of HFR under Transmission Cable Resistance Variation

In practical applications, the cable resistance parameter may always be in variation due to the temperature and humidity changing, insulation condition variation and etc. For the purpose of investigating the HFR performance under different cable resistance, the Nyquist diagram based method is adopted here.

Fig. 6 shows the Nyquist diagram of impedance ratio $Z_{unit(4)}/Z_{wf}$ between the transmission cable impedance and the DFIG wind farm impedance, thereafter the HFR can be accordingly identified. As shown in Fig. 6, it can be observed that as the cable resistance increases from 89.0 mΩ/km, to 133.5 mΩ/km and 178 mΩ/km, all the three Nyquist curves are very close to the point (-1,0), but not encircle the point, indicating the occurrence of the resonance, and the resonance exists in the steady state and does not results in divergence instability. Moreover, the phase margins of all three cases also increases from 1.2° to 2.4° and 3.6° respectively. Thus, it can be found out that the increasing of cable resistance is helpful to suppress the HFR by increasing the phase margin.

From the equivalent impedance point of view, the cable and DFIG system behave as almost pure capacitive and inductive respectively at the HFR frequency point. As a consequence, the amplitude of the HFR is mainly determined by the equivalent resistances included in both the cable impedance and the DFIG system impedance. The larger resistance (due to the larger phase margin shown in Fig. 6) indicates better damping of the HFR, i.e., smaller or even zero HFR amplitude. Thus, it can be found that the increasing of cable resistance helps to damp the HFR. Note that the potential HFR happens at 2035 Hz as shown in Fig. 6 due to the tiny stability margin, this conclusion will be verified by the following simulation results.

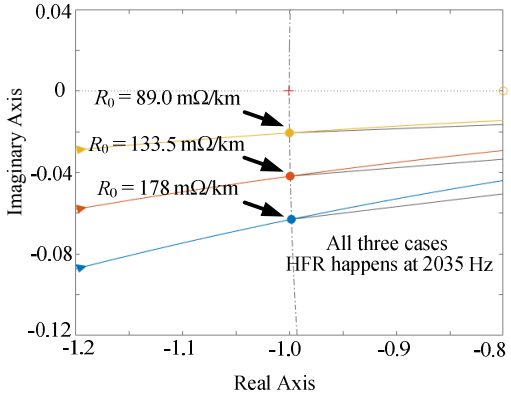

Fig. 6. Nyquist curve of the $Z_{unit(4)}/Z_{wf}$ under different cable resistance R_0 = 89.0, 133.5, 178 mΩ/km respectively

V. Simulation Validation

A. Simulation setup

In order to validate the HFR in the wind farm, a simulation model is built up, the control block is shown in Fig. 7, and the DFIG system parameters can be found in

Table I. The transmission cables are simulated as shown in Fig. 1 with their parameters listed in Table I. The rotor speed is set to 1200 rpm (0.8 p.u.), with the synchronous speed of 1500 rpm (1.0 p.u.). The dc-link voltage is 1200 V. The switching frequency f_{sw} for both RSC and GSC is 2.5 kHz, the sampling frequency f_s for both RSC and GSC is 5 kHz. The output wind power is set as 1.0 p.u. active power and 0.0 p.u. reactive power.

Since it is impossible to run the simulation based on MABLAB/Simulink with 200 single DFIG units, two single DFIG units are adopted here, while the impedance of the transmission cables are multiplied with 100 to represent the total number of 200 DFIG units, which finally build up a 400 MW wind farm.

B. Control block diagram

Fig. 7 shows the control block diagram of a single DFIG unit including the connection to the grid through long transmission cables. As it can be seen, for the RSC control, an Enhanced Phase Locked Loop (EPLL) is used to provide the information of grid voltage fundamental synchronous angular speed ω_1 and angle θ_1 information, while an encoder gives out the DFIG rotor position θ_r and speed ω_r. The rotor current $\boldsymbol{I}^{+}_{rdq}$ is first sampled and then controlled based on the reference value $\boldsymbol{I}^{+*}_{rdq}$ with a PI controller to output the harvested wind energy. The output of the rotor current PI closed-loop control $\boldsymbol{V}^{+}_{rdqPI}$ are added together with the decoupling compensation, giving out the rotor control voltage $\boldsymbol{V}^{+}_{rdq}$, which is then transformed to the rotor stationary frame and delivered as the input to the Space Vector Pulse Width Modulation (SVPWM).

As for the GSC control, the dc-link voltage V_{dc} is well regulated by a PI controller, and its output is delivered as the converter side inductance filter current reference $\boldsymbol{I}^{+*}_{fdq}$, which is used to regulate the actual converter side inductance filter current $\boldsymbol{I}^{+}_{fdq}$ by a PI controller. Similarly, the GSC control voltage $\boldsymbol{V}^{+}_{gdq}$ can be obtained by the PI current controller output and the decoupling compensation.

During the simulation validation, the transmission cable consists of 4 Π sections with the length of each section to be 5 km, thus the entire length of the cable is 20 km.

Fig. 8, Fig. 9 and Fig. 10 give out the simulation results of the DFIG wind farm connected to the transmission cable with the cable resistance R_0 = 89.0 mΩ/km, 133.5 mΩ/km and 178 mΩ/km respectively, both the DFIG system waveforms and the FFT analysis of the stator voltage are provided.

For the case of R_0 = 89.0 mΩ/km shown in Fig. 8, it can be observed that the significant amount of 79% high frequency resonance component at 2050 Hz in the stator voltage appears, and the stator current and the rotor current also inevitably contain this resonance components.

Moreover, for the case of R_0 = 133.5 mΩ/km shown in Fig. 9, the high frequency resonance component at 2050 Hz becomes smaller as 54% in the stator voltage due to the increasing of the cable resistance, and the stator current and the rotor current contain still the HFR as well.

Furthermore, for the case of R_0 = 178 mΩ/km shown in Fig. 10, the high frequency resonance component at 2050 Hz is smallest as 15 % among these three case studies due to the largest cable resistance. As a result, the stator current and the rotor current also become much sinusoidal compared with the other two cases.

Thus, by making comparison among these three simulation case studies, it can be concluded that,

1) The Nyquist diagram based method is capable of estimating the frequency of the HFR;

2) Larger cable resistance helps to mitigate the amplitude of the HFR, and even sinusoidal waveforms can be achieved if the cable resistance is sufficiently large;

3) The deviation of the cable resistance does not cause the HFR frequency shift, but only influence the HFR amplitude.

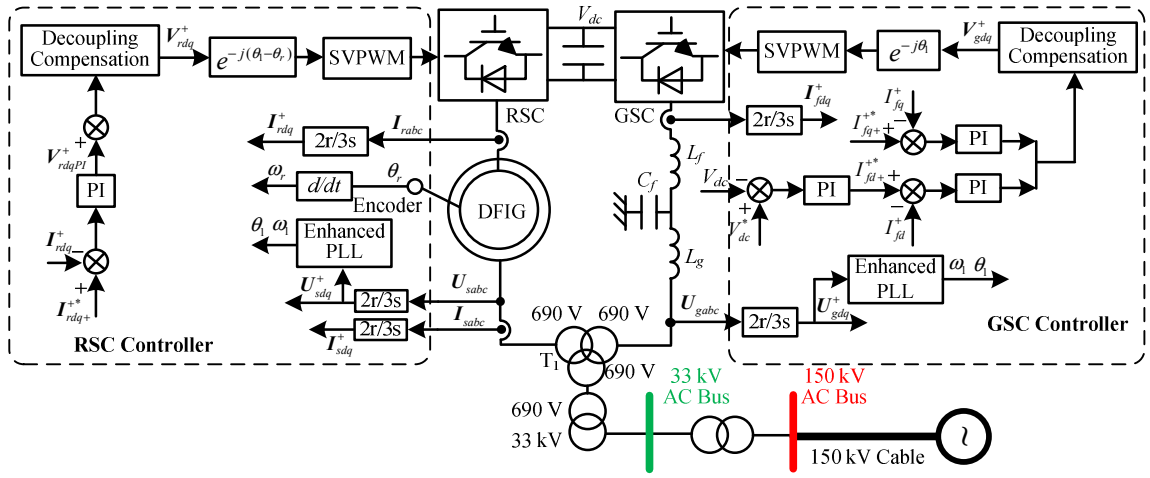

Fig. 7. Control block diagram of a single DFIG unit including the connection to the grid through long transmission cables

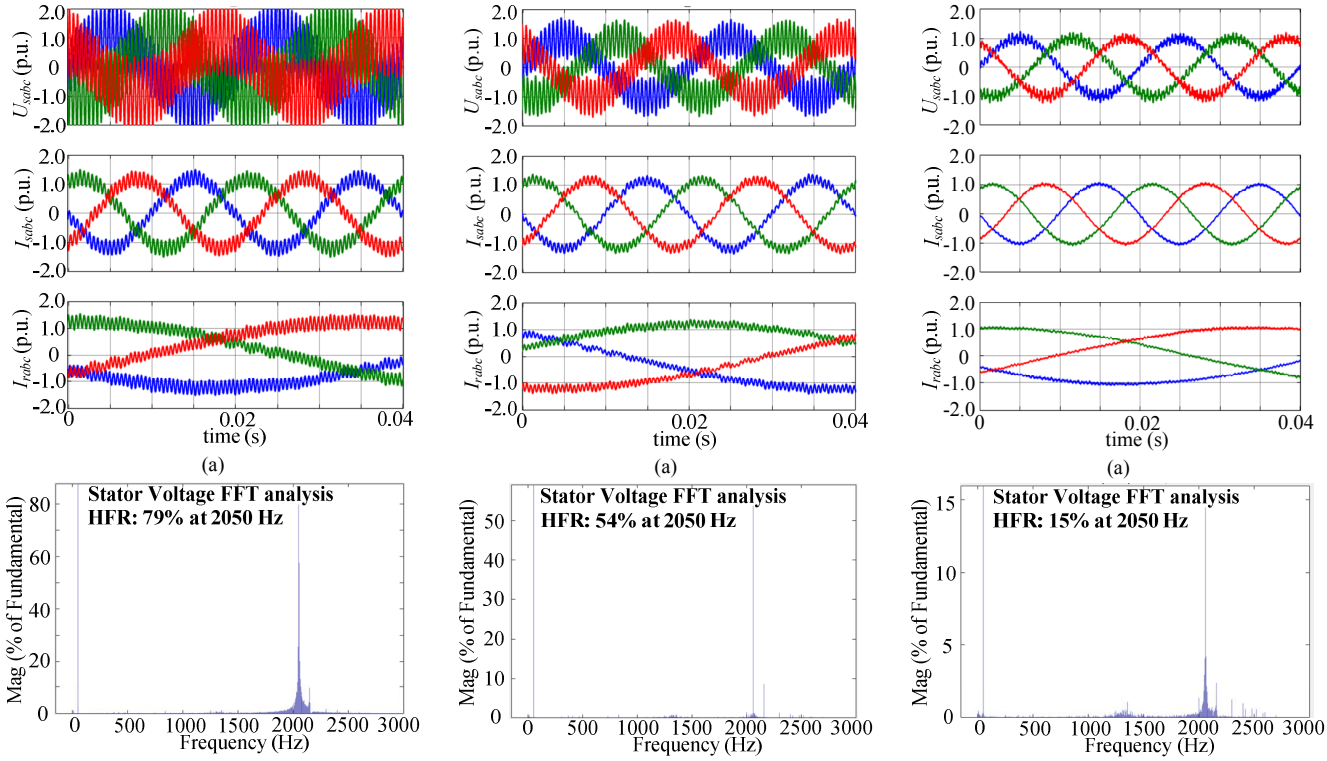

Fig. 8. Simulation results of DFIG wind farm connected to the transmission cable with cable resistance R_0 = 89.0 mΩ/km; (a) DFIG system waveforms; (b) FFT analysis of stator voltage

Fig. 9. Simulation results of DFIG wind farm connected to the transmission cable with cable resistance R_0 = 133.5 mΩ/km; (a) DFIG system waveforms; (b) FFT analysis of stator voltage

Fig. 10. Simulation results of DFIG wind farm connected to the transmission cable with cable resistance R_0 = 178 mΩ/km; (a) DFIG system waveforms; (b) FFT analysis of stator voltage

VI. Conclusions

This paper conducted the sensitivity analysis of the wind farm high frequency resonance under the variation of the transmission cable resistance, and the HFR can be identified using the method of Nyquist diagram. The variation of the cable resistance may occur in practical situation due to temperature changing and insulation conditions. It can be concluded that the increasing of cable resistance helps to suppress the amplitude of the HFR, but does not change the resonance frequency.

References

[1] J. Hu, B. Wang, W. Wang, H. Tang, Y. Chi, Q. Hu. "Small Signal Dynamics of DFIG-based Wind Turbines during Riding Through Symmetrical Faults in Weak AC Grid," *IEEE Trans. Energy Convers.*, vol. 32, no. 2, pp. 720–730, June 2017.

[2] J. Hu, L. Sun, X. Yuan, S. Wang, Y. Chi. "Modeling of Type 3 Wind Turbine with df/dt Inertia Control for System Frequency Response Study," *IEEE Trans. Power Systems*, vol. 32, no. 4, pp. 2799–2809, July 2017.

[3] H. Nian, P. Cheng, and Z. Q. Zhu, "Independent Operation of DFIG-Based WECS Using Resonant Feedback Compensators Under Unbalanced Grid Voltage Conditions," *IEEE Trans. Power Electron.*, vol. 30, no. 7, pp. 3650 - 3661, July 2015.

[4] H. Nian, P. Cheng, and Z. Q. Zhu, "Coordinated Direct Power Control of DFIG System Without Phase-Locked Loop Under Unbalanced Grid Voltage Conditions," *IEEE Trans. Power Electron.*, vol. 31, no. 4, pp. 2905 - 2918, April 2016.

[5] C. Wu, H. Nian, "Stator Harmonic Currents Suppression for DFIG Based on Feed-forward Regulator Under Distorted Grid Voltage," *IEEE Trans. Power Electron*., vol. 33, no. 2, pp. 1211–1224 , Feb. 2018.

[6] H. Nian, C. Wu, P. Cheng, "Direct Resonant Control Strategy for Torque Ripple Mitigation of DFIG Connected to DC Link through Diode Rectifier on Stator," *IEEE Trans. Power Electron*., vol. 32, no. 9, pp. 6936–6945 , Sept. 2017.

[7] H. Liu, J. Sun, "Voltage Stability and Control of Offshore Wind Farms With AC Collection and HVDC Transmission," *IEEE J. Emer. Sel. Topics Power Electron*., vol. 2, no. 4, pp. 1181 – 1189, Dec. 2014.

[8] Z. Miao, "Impedance-Model-Based SSR Analysis for Type 3 Wind Generator and Series-Compensated Network," *IEEE Trans. Energy Convers.*, vol. 27, no. 4, pp. 984–991, Dec. 2012.

[9] L. Piyasinghe, Z. Miao, J. Khazaei, and L. Fan, "Impedance Model-Based SSR Analysis for TCSC Compensated Type-3 Wind Energy Delivery Systems," *IEEE Trans. Sustainable Energy.*, vol. 6, no. 1, pp. 179–187, Jan. 2015.

[10] L. Fan, and Z. Miao, "Nyquist-Stability-Criterion-Based SSR Explanation for Type-3 Wind Generators," *IEEE Trans. Energy Convers.*, vol. 27, no. 3, pp. 807–809, Sep. 2012.

[11] L. Fan, and Z. Miao, "Mitigating SSR Using DFIG-Based Wind Generation," *IEEE Trans. Sustainable Energy.*, vol. 3, no. 3, pp. 349–358, July 2012.

[12] Y. Song, F. Blaabjerg, "Analysis on the Behavior of Undamped and Unstable High Frequency Resonance in DFIG System," *IEEE Trans. Power Electron*., vol. 32, no. 12, pp. 9105-9116, Dec. 2017.

[13] Y. Song, X. Wang, F. Blaabjerg, "Impedance-Based High Frequency Resonance Analysis of DFIG System in Weak Grids," *IEEE Trans. Power Electron*., vol. 32, no. 5, pp. 3536-3548, May 2017.
[14] Z. Chen, A. Luo, H. Kuang, L. Zhou, Y. Chen, Y. Huang, "Harmonic resonance characteristics of large-scale distributed power plant in wideband frequency domain," *Electric Power Systems Research*, vol. 143, pp. 53-65, 2017.
[15] J. Sun, "Impedance-Based Stability Criterion for Grid-Connected Inverters," *IEEE Trans. Power Electron*., vol. 26, no. 11, pp. 3075 - 3078 Nov. 2011.
[16] I. Vieto, and J. Sun, "Damping of Subsynchronous Resonance Involving Type-III Wind Turbines," *in Proc. Control and Modeling for Power Electronics* (COMPEL), pp. 1-8, 2015.
[17] I. Vieto, and J. Sun, "Small-Signal Impedance Modeling of Type-III Wind Turbine," *in Proc. Power & Energy Society General Meeting* (PESG), pp. 1-5, 2015.
[18] I. Vieto, and J. Sun, "Real-time Simulation of Subsynchronous Resonance in Type-III Wind Turbines," *in Proc. Control and Modeling for Power Electronics* (COMPEL), pp. 1-8, 2014
[19] I. Vieto, and J. Sun, "Sequence Impedance Modeling and Analysis of Type-III Wind Turbines," *IEEE Trans. Energy Convers.*, early access.